Ann Nucl Med (2017) 31:529–535
DOI 10.1007/s12149-017-1177-0

ORIGINAL ARTICLE

Characteristics of single- and dual-photopeak energy window acquisitions with thallium-201 IQ-SPECT/CT system

Takayuki Shibutani[1,2] · Masahisa Onoguchi[1] · Hiroto Yoneyama[3] · Takahiro Konishi[3] · Shinro Matsuo[4] · Kenichi Nakajima[2,4] · Seigo Kinuya[2,4]

Received: 7 February 2017 / Accepted: 25 April 2017 / Published online: 3 May 2017

Abstract
Objectives Although dual-energy (DE) acquisition with conventional ^{201}Tl myocardial perfusion SPECT has several advantages such as improved attenuation of the inferior wall and increased acquisition counts, the characteristics of IQ-SPECT have not been fully evaluated. We evaluate the difference of characteristics between single-energy (SE) and dual-energy (DE) imaging using ^{201}Tl myocardial IQ-SPECT.
Methods Two myocardial phantoms were created simulating normal myocardium and infarction of the inferior wall. Energy windows were set at 70 keV ± 10% for SE, and an additional 167 keV ± 7.5% for DE. SPECT images were reconstructed using the ordered subset conjugates gradient minimizer (OSCGM) method. We visually and quantitatively compared short-axis images of correction for no (NC), for attenuation (AC) or for both AC and scatter (ACSC) images.
Results The average counts of SE and DE projection data were 17.5 and 20.3 counts/pixel, respectively. The DE data increased acquisition counts by approximately 16% compared with the SE data. The average visual score of normal myocardium did not differ significantly between the SE and DE images. However, the DE image of defective myocardium showed a significantly lower score in AC than SE images. The % uptake values of DE image with both NC and AC were significantly higher than those of SE images. The DE images of the inferior defective areas (segments 4 and 10) showed approximately 5–10% higher uptake compared with the SE images.
Conclusion The DE image with NC improved attenuation of the inferior wall. However, DE image with AC showed low defect detectability. Thus, AC should be used with SE rather than DE. Furthermore, while the SE image with ACSC can be used to detect perfusion defects, it must be interpreted carefully including the possibility of artificial inhomogeneity even in the normal myocardium.

Keywords IQ-SPECT · ^{201}Tl myocardial perfusion SPECT · Energy window · Computed tomography-based attenuation correction · Phantom study

Introduction

Myocardial perfusion single-photon emission computed tomography (SPECT) with ^{201}Tl is widely used for diagnosis of myocardial ischemia, indication of revascularization, and therapeutic evaluation [1–5]. The ^{201}Tl emits two γ-rays of 135 (2.6%) and 167 (10.0%) keV, and a characteristic X-ray of 69–83 (94.1%) keV with Hg-201 by electron capture disintegration. The ^{201}Tl myocardial imaging is acquired using either a single-energy (SE) window setting with a characteristic X-ray peak of 69–83 keV or a dual-energy (DE) window setting with additional γ-rays of 167 keV. Myocardial images of DE window using a low-energy high-resolution (LEHR)

✉ Masahisa Onoguchi
onoguchi@staff.kanazawa-u.ac.jp

1 Department of Quantum Medical Technology, Institute of Medical, Pharmaceutical and Health Sciences, Kanazawa University, Kanazawa, Japan

2 Department of Nuclear Medicine, Graduate School of Medical Science, Kanazawa University, Kanazawa, Japan

3 Department of Radiological Technology, Kanazawa University Hospital, Kanazawa, Japan

4 Department of Nuclear Medicine, Kanazawa University Hospital, Kanazawa, Japan

collimator have reported the utility for adding myocardial counts and improving inferior attenuation artifact [6, 7]. Furthermore, Seo et al. reported that μ values to perform attenuation correction (AC) for DE can be calculated from the percentage of two emitted different energies [8]. Thus, the DE images for ^{201}Tl myocardial SPECT have several advantages.

IQ-SPECT is a highly sensitive myocardial perfusion SPECT using multifocal collimators that can reduce scan time compared with conventional SPECT with a parallel-hole collimator [9]. The multifocal collimator to magnify the heart with a cardio-centric acquisition method, along with a reconstruction technique based on the conjugate gradient method, enhanced the clinical use of this device [9–11]. While ^{201}Tl myocardial perfusion imaging has been reported to be clinically feasible using the IQ-SPECT system [12–15], the studies used only SE images, and characteristics of DE images for IQ-SPECT have not yet been evaluated. The aim of this study was to evaluate the difference of characteristics between SE and DE imaging using ^{201}Tl myocardial IQ-SPECT.

Materials and methods

Phantom designs

An anthropomorphic phantom featuring inserts to simulate lungs, liver, left ventricular (LV) wall, and LV chamber (Data spectrum Corp., Durhan, NC, USA) was used in this study. Two myocardial phantoms were created simulating normal myocardium and myocardial infarction. The myocardial defect was filled with nonradioactive water to simulate a transmural defect with rectangular shapes (major axis, 30 mm; minor axis, 20 mm) and located in the mid to basal inferior position in the LV wall (Fig. 1). The lung inserts were filled with Styrofoam beads. Myocardium and liver were filled with variable concentrations of ^{201}Tl, and the radioactive concentration was 61.8 kBq/mL for myocardium, 37.1 kBq/mL for the liver and 4.9 kBq/mL for the chest. The LV chamber was filled with nonradioactive water.

Acquisition protocols and image reconstruction parameters

IQ-SPECT was acquired on a hybrid dual-head SPECT/CT system (Symbia T6, Siemens, Tokyo, Japan) equipped with multifocal collimators (SMARTZOOM) of 128 × 128 matrix size, pixel size of 4.8 mm and a zoom factor of one. Spatial resolution is progressively increased from the camera surface to the cardiac sweet-spot at 28 cm, which was set as the center of rotation for this study, thereby keeping the LV phantom at the highest magnification throughout the acquisition. The two detectors were in a 76° configuration, with a scan arc of 104° acquired from the right anterior oblique (RAO) 59° to left posterior oblique (LPO) 59° with 6° angular steps. For each detector, 17 views were acquired, and acquisition time was 14 s/view. Energy windows were set at 70 keV ± 10% for SE, and an additional 167 keV ± 7.5% for DE. Scatter energy windows were set at 20% lower and upper for 70 keV. The computed tomography (CT) scanning parameters were slice thickness of 5 mm, tube voltage of 130 kVp, tube current–time of 20 mAs, rotation speed of 0.6 s per rotation, and scan pitch of 1.0 mm.

Acquired data were reconstructed using the ordered subset conjugates gradient minimizer (OSCGM) method. Subsets and iterations were 3 and 13, respectively. A Gaussian filter (full width at half maximum: FWHM 9.6 mm) was used as a post filter. The triple energy window method was used for SC. AC was applied using a patient-dedicated low-dose CT-derived μ map for SE and DE. However, this method must be modified to calculate an attenuation map for DE. Therefore, we calculated from a technique used by Seo et al. [8], in which the effective attenuation coefficient for photons of 2 different energies from a single radionuclide is expressed by:

$$\mu_{\mathrm{eff}} = \frac{\mathrm{In}[\exp(-\mu_1 x) + \alpha \exp(-\mu_2 x)] - \mathrm{In}(1+\alpha)}{-x}.$$

where μ_1 and μ_2 are attenuation coefficients for 70 and 167 keV, α is the ratio of the branching ratios, and x is the thickness of the medium through which the x- and γ-rays pass. The linear attenuation coefficients μ_1 and μ_2 also are obtained from tabulated values, with α calculated from the branching ratios (i.e., 90.22%, 9.78%) of the 70 keV X-ray and 167 keV γ-ray (i.e., $\alpha = 90.22\%/9.78\% = 9.22$) [8, 16]. The effective linear attenuation coefficient of effective energy is relatively constant as a function of object thickness x, thereby producing an attenuation map at a single effective energy at $E_{\mathrm{eff}} = 79$ keV that can be applied to pooled data acquired from ^{201}Tl [16].

Three kinds of myocardial images were created, namely (1) no correction (NC) without scatter correction (SC) and AC, (2) with AC, and (3) with both AC and SC (ACSC), while DE image with ACSC could not be created due to the system limitation.

Image assessment

We manually drew regions of interest (ROI) on the lateral myocardium for the left anterior oblique (LAO) 45° of both SE and DE projection data, and the average counts in ROI were calculated. Reconstructed SE and DE short-axis images for the normal and inferior defective myocardium

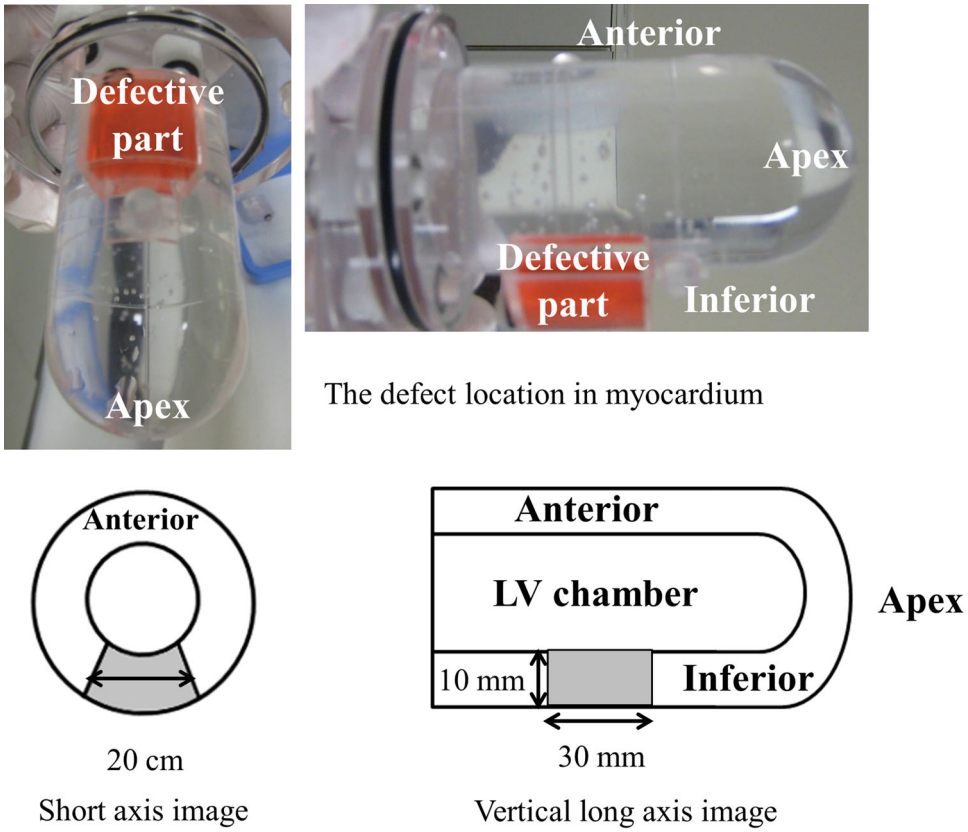

Fig. 1 The structure of myocardial phantom with an inferior defect. The myocardial defect was filled with nonradioactive water to simulate a transmural defect of *rectangular shape* (major axis, 30 mm; minor axis, 20 mm) and located in the mid to basal inferior position in the left ventricular wall. The *upper and lower images* were phantom picture and design of transmural defect location

were assessed visually for image quality using a five-point (5, excellent; 4, good; 3, even; 2, bad; 1, poor) scale by four observers. Furthermore, we created a 17-segment polar map [17] and quantitatively assessed using percent uptake (% uptake) of each segment with the normal myocardium. We also calculated the coefficient of variation (CV) using % uptake on a 17-segment polar map. In the defective myocardium, average % uptake values of mid and basal inferior walls (segments 4 and 10) were calculated.

Statistical analysis was performed using statistical package for social science (SPSS) software (version 21 for Windows, SPSS Inc., Chicago, IL, USA). Visual score of the normal and defective myocardium was evaluated by the Mann–Whitney *U* test. The % uptake of each segment with normal myocardium was examined by paired *t* and Bonferroni after Friedman tests. p value <0.05 was considered to be statistically significant.

Results

The average counts/pixel for SE and DE projection data were 17.5 and 20.3, respectively. The acquisition counts were increased in DE data by approximately 16% compared with the SE data. Figure 2 shows SE and DE images of the normal and the inferior defective myocardium using NC, AC, and ACSC. The DE image with NC improved % uptake of the inferolateral area compared with the SE image in normal myocardium, resulting in more homogeneous uptake in the DE image. In the DE image with AC, the inferior defect was not so obvious compared with the SE image. The average visual scores of normal myocardium for both SE and DE images were 3.9 ± 0.2 and 4.4 ± 0.3 with NC, 4.5 ± 0.3 and 4.7 ± 0.3 with AC, and 3.8 ± 0.3 with SE of ACSC, respectively (Fig. 3). However, myocardial images of both NC and AC did not differ significantly between the SE and DE images. In addition, the SE images with ACSC showed lower score than that with AC, whereas the visual homogeneity score of the SE image showed no significant difference between AC and ACSC ($p = 0.20$). The average visual score of inferior defective myocardium for both SE and DE images were 4.8 ± 0.3 and 4.5 ± 0.3 with NC, 5.0 ± 0 and 2.0 ± 0.4 with AC, and 4.8 ± 0.3 with SE of ACSC, respectively (Fig. 4). The DE image showed significantly lower score in AC than SE image ($p = 0.029$), whereas the visual defect score of the SE image showed no significant difference between AC and ACSC ($p = 0.69$). Figure 5 shows % uptake of each segment for the normal myocardium. The median % uptake values (minimum–maximum values) of SE and DE image

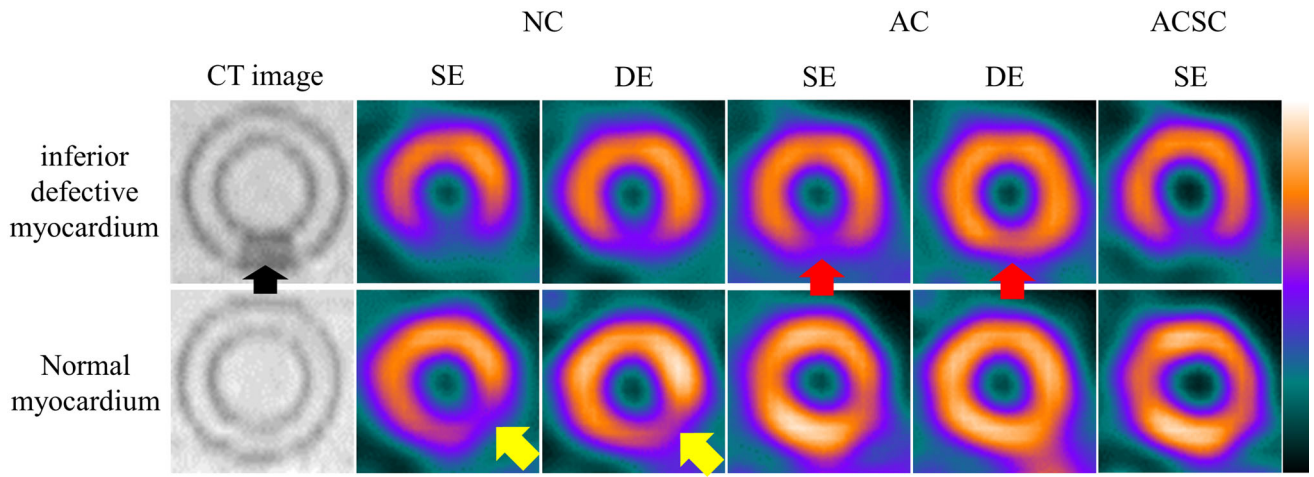

Fig. 2 The single-energy (SE) and dual-energy (DE) images of both normal and the inferior defective myocardium among no correction (NC), attenuation correction (AC) and both attenuation and scatter corrections (ACSC). The *left image* shows the CT image of the normal and defective myocardium as a reference. The *upper and lower row images* show inferior defective and normal myocardium, respectively. The DE image with NC improved % uptake of inferolateral area compared with the SE image in normal myocardium, resulting in more homogeneous uptake in the DE image (*yellow arrow*). In the DE image with AC, the inferior defect was not so obvious, rather than in the SE image, due to over-correction of attenuation (*red arrow*)

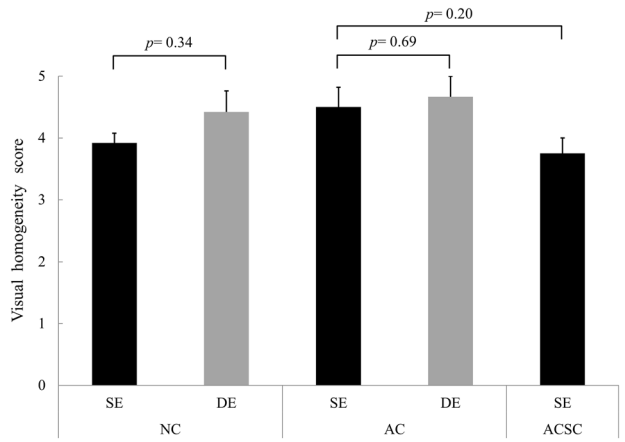

Fig. 3 Visual homogeneity score of both single-energy (SE) and dual-energy (DE) images for the normal myocardium. *NC* no correction, *AC* attenuation correction, *ACSC* both attenuation and scatter corrections

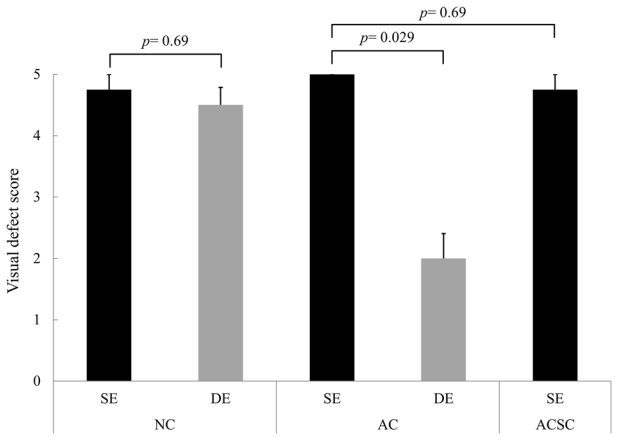

Fig. 4 Visual defect score of both single-energy (SE) and dual-energy (DE) images for the inferior defective myocardium. *NC* no correction, *AC* attenuation correction, *ACSC* both attenuation and scatter corrections

for all segments were 72.4% (58.5–90.1%) and 76.0% (62.8–94.0%) with NC, 81.0% (70.6–89.9%) and 89.2% (73.1–96.1%) with AC, and 80.4% (67.3–89.8%) with SE of ACSC, respectively. The % uptake of DE images for all segments was significantly higher than that of SE images with both NC and AC ($p = 0.002$ with NC and $p < 0.001$ with AC). Furthermore, the % uptake of SE images with AC has significantly higher than that with NC for all segments. However, the % uptake of AC and ACSC did not differ significantly ($p = 0.03$, NC versus AC and $p = 0.12$, AC versus ACSC). The CVs of both SE and DE images were 0.14 and 0.12 for NC, 0.08 and 0.07 for AC, and 0.09 with SE of ACSC, respectively. The DE images showed higher uniformity than that of SE images with both NC and AC.

The median % uptake of the inferior defective areas (segments 4 and 10) for both SE and DE images were 50.4 and 54.9 with NC, 68.5 and 76.7 with AC, and 65.3 with SE of ACSC, respectively (Fig. 6). The DE images showed approximately 5–10% higher % uptake compared with the SE images.

Discussion

Conventional myocardial perfusion SPECT for ^{201}Tl requires acquisition time of 20–25 min. Since patients are asked to remain in supine position with both arms raised above the head, many patients may suffer pain and cause

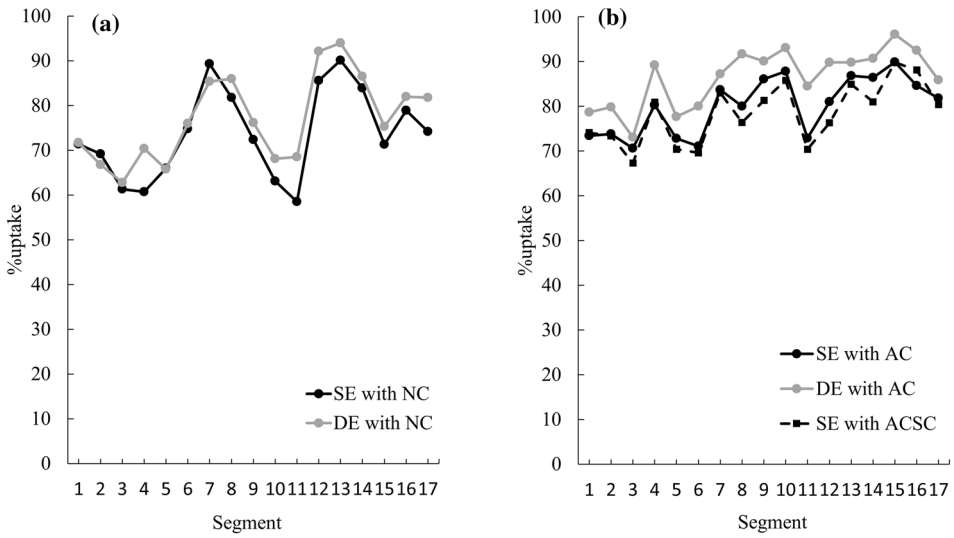

Fig. 5 The % uptake values of single-energy (SE) and dual-energy (DE) images for normal myocardium with a 17-segment polar map by NC (**a**) and both AC and ACSC (**b**). *NC* no correction, *AC* attenuation correction, *ACSC* both attenuation and scatter corrections

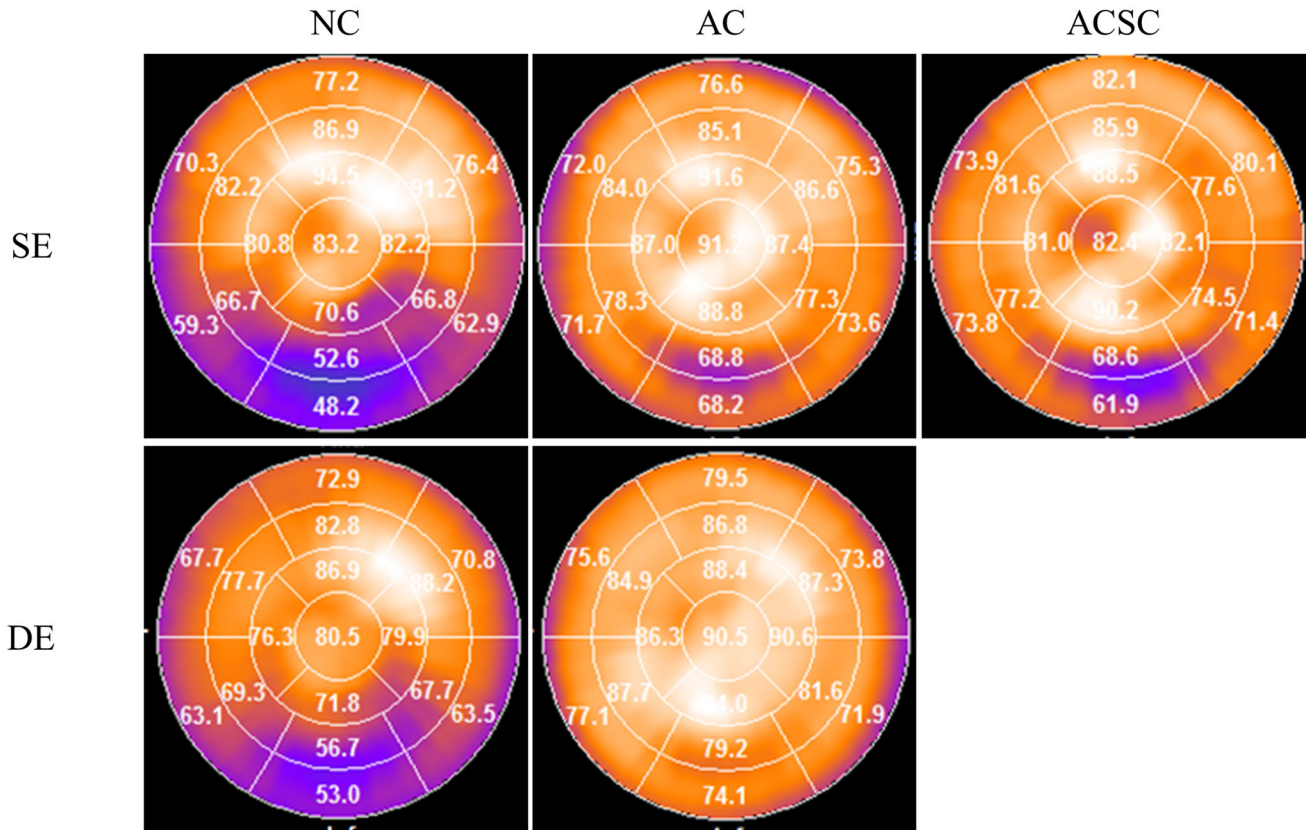

Fig. 6 The polar map of single-energy (SE) and dual-energy (DE) images for the inferior defective myocardium. *NC* no correction, *AC* attenuation correction, *ACSC* both attenuation and scatter corrections

the motion artifact [18, 19]. Therefore, shorter acquisition time is beneficial to improve pain palliation in patients and reducing patient motion. Recently, to shorten acquisition time, researchers have reported acquisition protocols and image processing technology [9, 20–22]. IQ-SPECT for ^{201}Tl can acquire images with shorter time in comparison with conventional SPECT, which have been used successfully for diagnosis [12–14]. However, preceding studies have evaluated only SE image, and characteristics of DE images for IQ-SPECT have not been evaluated. The DE image for ^{201}Tl myocardial perfusion SPECT has increased myocardial counts and improved inferior attenuation artifact compared with conventional SPECT using LEHR collimator [6, 7]. Therefore, we

aimed to reveal characteristics of DE images for IQ-SPECT.

The DE data increased acquisition counts by approximately 16% in comparison with SE data, thereby higher myocardial counts can be obtained, which is the similar tendency to the previous study [6, 7]. The OSCGM algorithm is increased approximately 1000-fold counts in the pixel using scaling factor. In this study, the acquisition counts of DE data increased a few counts comparing with SE data. However, the difference of few counts after the decimal number have an influence on image quality by the effect of scaling factor, and increased acquisition counts can improve the image quality by decreasing statistical noise. Furthermore, the counts level of nuclear medicine imaging has an important role in diagnosis accuracy, which potentially leads to accurate diagnosis [23]. In this regards, the DE acquisition is convenient for increasing myocardial counts.

In ^{201}Tl myocardial perfusion SPECT, artifacts may occur in the anterior or inferior walls due to breast in women or diaphragmatic attenuations in men, which may decrease diagnosis accuracy [24]. However, diagnostic accuracy could enhance by changing radiopharmaceutical agent from ^{201}Tl to ^{99m}Tc and additional acquisition of prone-position imaging [15, 25]. These improvements are important but have some limitations such as modification of acquisition protocol or extension of examination time. When comparing SE and DE images, the DE image of normal myocardium has slightly higher % uptake and lower CV than the SE image. In particular, the % uptake of the inferoseptal (segments 3 and 9) and inferior (segments 4 and 10) walls of DE images was increased by 2–10% both NC and AC. Therefore, the DE image for IQ-SPECT can improve artifact of inferoseptal and inferior walls without changing radiopharmaceutical agent or additional acquiring prone-position, as previously reported [6, 7]. The SE images for IQ-SPECT showed lower % uptake of approximately 10–12% for the inferolateral walls (segment 11) than the DE image with both NC and AC, and this is characteristic of IQ-SPECT system as reported [26]. On the other hand, the DE image could improve artificial low counts of the inferolateral wall. In particular, DE image with NC will be useful for improving the artifact such as attenuation of inferoseptal and inferior walls. However, the DE image with AC significantly decreased defect detectability in this study. The scattered activity from the liver with DE image is higher than that with SE image, and the inferior wall is liable to be affected by the scatter from the liver. In the DE image, therefore, the inferior wall activity is overcorrected due to scattered activity from the liver in the AC image without SC, which resulted in lower detectability of the defect. Furthermore, we visually and quantitatively evaluated inferior defect detectability using the myocardial phantom. Since the effect of scatter and attenuation is the highest in the inferior wall, we focused our study on the phantom with the inferior defect with AC and SC. Therefore, we considered that the inferior defect was appropriate for evaluating the effect of AC and SC. The defect parts (segments 4 and 10) of SE images with ACSC showed 0.2–6.3% lower uptake than that with AC, which is close to the theoretical value (% uptake = 0) of the transmural defect. In principle, the SPECT image should incorporate both attenuation and scatter correction. Since the SE image with ACSC showed nearly equivalent image quality compared with the SE images with AC, we would like to recommend the SE image with ACSC.

In summary, we recommend either DE with NC for IQ-SPECT system unequipped CT or SE with ACSC for IQ-SPECT/CT system in ^{201}Tl myocardial IQ-SPECT. If IQ-SPECT unequipped with CT device is used, since the patient attenuation cannot be corrected by CT, DE image with NC will be useful to improve the inferior wall attenuation.

Finally, appropriate normal databases should be provided for quantitative analysis of myocardial perfusion imaging, although Japanese Society of Nuclear Medicine working group has created normal databases for ^{201}Tl IQ-SPECT imaging [27]. In this database, CT-based attenuation correction was performed with an SE method. The influence of SE and DE acquisition on the diagnostic accuracy in clinical settings should be further investigated.

We could not create the DE images with ACSC due to the limitation of energy window setting, and could not compare the SE and DE images with ACSC. If the limitation is improved, the potential usefulness of DE images with ACSC should be further investigated. However, the SE image with ACSC showed nearly equivalent image quality compared with the SE images with AC and the DE image with NC. Therefore, the SE image with ACSC will be useful in diagnosis as previously described [12–15].

Conclusion

We evaluated the difference of characteristics between SE and DE imaging using ^{201}Tl myocardial IQ-SPECT. The DE image with NC was useful for improving the artifact such as attenuation of the inferoseptal and inferior walls, which is sometimes difficult to differentiate from true defect in the inferolateral wall. Since the defect detectability of DE image with AC significantly decreased, the SE image of ACSC is recommended for excellent image quality.

Acknowledgements The authors thank Go Omori, RT at Sapporo medical university hospital for support of technical experience.

Compliance with ethical standards

Conflict of interest K. Nakajima has a collaborative research work with Siemens Japan (Tokyo, Japan). Other authors report no potential conflicts of interest relevant to this study.

References

1. Nishimura S, Mahmarian JJ, Boyce TM, Verani MS. Quantitative thallium-201 single-photon emission computed tomography during maximal pharmacologic coronary vasodilation with adenosine for assessing coronary artery disease. J Am Coll Cardiol. 1991;18:736–45.
2. Takao Y, Murata H, Katoh K. Availability and limitations of thallium-201 myocardial SPECT quantitative analysis: assessment as daily routine procedure for ischemic heart disease. Ann Nucl Med. 1991;5:11–8.
3. Tamaki N, Yonekura Y, Mukai T, Kodama S, Kadota K, Kambara H, et al. Stress thallium-201 transaxial emission computed tomography: quantitative versus qualitative analysis for evaluation of coronary artery disease. J Am Coll Cardiol. 1984;4:1213–21.
4. Caymaz O, Fak AS, Tezcan H, Inanir S, Toprak A, Tokay S, et al. Correlation of myocardial fractional flow reserve with thallium-201 SPECT imaging in intermediate-severity coronary artery lesions. J Invasive Cardiol. 2000;12:345–50.
5. Yanagisawa H, Chikamori T, Tanaka N, Hatano T, Morishima T, Hida S, et al. Correlation between thallium-201 myocardial perfusion defects and the functional severity of coronary artery stenosis as assessed by pressure-derived myocardial fractional flow reserve. Cir J. 2002;66:1105–9.
6. Hansen CL, Siegel JA. Attenuation correction of thallium SPECT using differential attenuation of thallium photons. J Nucl Med. 1992;33:1574–7.
7. Brown JK, Tang HR, Hattner RS, Bocher M, Ratzlaff NW, Kadkade PP, et al. Intrinsic dual-energy processing of myocardial perfusion images. J Nucl Med. 2000;41:1287–97.
8. Seo Y, Wong KH, Sun M, Franc BL, Hawkins RA, Hasegawa BH. Correction of photon attenuation and collimator response for a body-contouring SPECT/CT imaging system. J Nucl Med. 2005;46:868–77.
9. Vija AH, Malmin R, Yahil A, Zeintl J, Bhattacharya M, Rempel TD, et al. A method for improving the efficiency of myocardial perfusion imaging using conventional SPECT and SPECT/CT imaging systems. In: IEEE nuclear science symposium and medical imaging conference record; 2010, pp. 3433–7.
10. Zeintl J, Rempel TD, Bhattacharya M, Malmin RE, Vija AH. Performance characteristics of the SMARTZOOM® collimator. In: Nuclear science symposium and medical imaging conference (NSS/MIC) IEEE; 2011, pp. 2426–9.
11. Onoguchi M, Konishi T, Shibutani T, Matsuo S, Nakajima K. Technical aspects: image reconstruction. Ann Nucl Cardiol. 2016;2:68–72.
12. Matsuo S, Nakajima K, Onoguchi M, Wakabayash H, Okuda K, Kinuya S. Nuclear myocardial perfusion imaging using thallium-201 with a novel multifocal collimator SPECT/CT: IQ-SPECT versus conventional protocols in normal subjects. Ann Nucl Med. 2015;29:452–9.
13. Takahashi T, Tanaka H, Kozono N, Tanakamaru Y, Idei N, Ohashi N, et al. Characteristics of images of angiographically proven normal coronary arteries acquired by adenosine-stress thallium-201 myocardial perfusion SPECT/CT-IQ SPECT with CT attenuation correction changed stepwise. Ann Nucl Med. 2015;29:256–67.
14. Horiguchi Y, Ueda T, Shiomori T, Kanna M, Matsushita H, Kawaminami T, et al. Validation of a short-scan-time imaging protocol for thallium-201 myocardial SPECT with a multifocal collimator. Ann Nucl Med. 2014;28:707–15.
15. Takamura T, Horiguchi Y, Kanna M, Matsushita H, Sudo Y, Kikuchi S, et al. Validation of prone myocardial perfusion SPECT with a variable-focus collimator versus supine myocardial perfusion SPECT with or without computed tomography-derived attenuation correction. Ann Nucl Med. 2015;29:890–6.
16. Seo Y, Wong KH, Hasegawa BH. Calculation and validation of the use of effective attenuation coefficient for attenuation correction in In-111 SPECT. Med Phys. 2005;32:3628–35.
17. Cerqueira MD, Weissman NJ, Dilsizian V, Jacobs AK, Kaul S, Laskey WK, et al. Standardized myocardial segmentation and nomenclature for tomographic imaging of the heart. A statement for healthcare professionals from the Cardiac Imaging Committee of the Council on Clinical Cardiology of the American Heart Association. Circulation. 2002;105:539–42.
18. Toma DM, White MP, Mann A, Phillips JM, Pelchat DA, Giri S, et al. Influence of arm positioning on rest/stress technetium-99m labeled sestamibi tomographic myocardial perfusion imaging. J Nucl Cardiol. 1999;6:163–8.
19. Cooper JA, Neumann PH, McCandless BK. Effect of patient motion on tomographic myocardial perfusion imaging. J Nucl Med. 1992;33:1566–71.
20. DePuey EG, Bommireddipalli S, Clark J, Leykekhman A, Thompson LB, Friedman M. A comparison of the image quality of full-time myocardial perfusion SPECT vs wide beam reconstruction half-time and half-dose SPECT. J Nucl Cardiol. 2011;18:273–80.
21. Asao K, Takaki A, Tominaga M, Sasaki M. The interpolated projection data estimation method improves the image quality of myocardial perfusion SPECT with a short acquisition time. Ann Nucl Med. 2012;26:123–30.
22. De Lorenzo A, Fonseca LM, Landesmann MC, Lima RS. Comparison between short-acquisition myocardial perfusion SPECT reconstructed with a new algorithm and conventional acquisition with filtered backprojection processing. Nucl Med Commun. 2010;31:552–7.
23. He X, Links JM, Frey EC. An investigation of the trade-off between the count level and image quality in myocardial perfusion SPECT using simulated images: the effects of statistical noise and object variability on defect detectability. Phys Med Biol. 2010;55:4949–61.
24. Desmarais RL, Kaul S, Watson DD, Beller GA. Do false positive thallium-201 scans lead to unnecessary catheterization? Outcome of patients with perfusion defects on quantitative planar thallium-201 scintigraphy. J Am Coll Cardiol. 1993;21:1058–63.
25. Wang SJ, Chen YT, Hwang CL, Lin MS, Kao CH, Yeh SH. ^{99m}Tc-sestamibi can improve the inferior attenuation of TL-201 myocardial spect imaging. Int J Card Imaging. 1993;9:87–92.
26. Caobelli F, Kaiser SR, Thackeray JT, Bengel FM, Chieregato M, Soffientini A, et al. IQ SPECT allows a significant reduction in administered dose and acquisition time for myocardial perfusion imaging: evidence from a phantom study. J Nucl Med. 2014;55:2064–70.
27. Nakajima K, Matsumoto N, Kasai T, Matsuo S, Kiso K, Okuda K. Normal values and standardization of parameters in nuclear cardiology: Japanese Society of Nuclear Medicine working group database. Ann Nucl Med. 2016;30:188–99.